

RESEARCH ON EFFECTIVENESS-DRIVEN INTELLIGENT OPTIMIZATION METHOD FOR CONCEPTUAL LAYOUT OF AIRCRAFT

Wenzheng Liu[1,2], Bolin Shang[1,2,3], Pengfei Li[1,2], Renxiang Ling[1,2], Yaozu Wang[1,2], Keao Xing[1,2], Hongxing Li[1,2]& Mingzhu Hou[1,2]

[1]School of Aeronautics, Northwestern Polytechnical University, Xi'an 710072, China
[2]National Key Laboratory of Aircraft Configuration Design, Xi'an 710072, China
[3] Key Laboratory of Aircraft System of Systems Contribution and Synthetic Design, Ministry of Industry and Information Technology, Xi'an 710072, China

Abstract

Modern air combat is shifting from performance confrontation between individual weapon platforms to effectiveness confrontation between systems-of-systems. This imposes new requirements on aircraft conceptual design: rather than purely pursuing optimal platform performance, the goal is to enable the aircraft to maximize the overall effectiveness of the air combat system-of-systems in which it operates. To address this need, this paper proposes an effectiveness-driven intelligent optimization method for the conceptual layout of air combat equipment. Aiming at maximizing air combat system-of-systems effectiveness, the method constructs a cross-level optimization framework of "layout parameters – aircraft performance – system-of-systems effectiveness," integrating parametric modeling, empirical engineering formulas, Agent-based system-of-systems simulation, and an improved genetic algorithm to form a closed-loop process of "design – simulation – optimization." First, a rapid estimation model that fuses subsonic flight performance and radar stealth performance is established. Then, based on the ABMS (Agent-Based Modeling and Simulation) concept, a repeatable and controllable air combat system-of-systems confrontation simulation platform is built. Finally, a typical mission scenario of fighters escorting bombers to conduct air-to-surface strikes is used as a case study for validation. The results show that the method can automatically iterate and optimize the equipment conceptual layout to achieve optimal system-of-systems effectiveness, and the resulting layout scheme achieves an effective balance between stealth and flight performance, validating the feasibility and effectiveness of the proposed method.

Keywords: air combat system-of-systems; conceptual layout; effectiveness-driven; genetic algorithm; simulation optimization

1. General Introduction

With the rapid development of technologies such as communications, networking, and cooperative engagement, modern warfare has evolved from traditional "platform-centric warfare" into system-of-systems confrontation. Against this backdrop, the design philosophy of weapon equipment is undergoing profound changes: shifting from previously emphasizing the performance metrics of individual weapon platforms—such as flight speed, maneuverability, and firepower—to pursuing the maximization of the overall operational effectiveness of the entire combat system-of-systems. As Sproles pointed out, the measurement of effectiveness must be based at the system-of-systems level and cannot be limited merely to the technical parameters of individual systems [1]. Therefore, how to optimize aircraft design driven by air combat system-of-systems effectiveness, and how to ensure that aircraft design schemes can maximize system-of-systems effectiveness to the greatest extent, have become critical issues urgently requiring breakthroughs in the field of aviation equipment systems.

In the conceptual layout design phase of aircraft, traditional optimization methods primarily rely on Multidisciplinary Design Optimization (MDO) techniques and expert experience. MDO methods integrate multiple disciplines such as aerodynamics, structures, and control into a unified whole to characterize the mutual coupling effects among various factors [2][3]. Building on this, Uncertainty-based Multidisciplinary Design Optimization (UMDO) further introduces the analysis of uncertain factors such as manufacturing errors and environmental fluctuations, in order to seek more robust and reliable optimal solutions [4][5]. However, the optimization objectives of such methods have always been confined to the performance metrics of the aircraft platform itself—such as lift-to-drag ratio, structural weight, and range—without comprehensively considering the aircraft and the air combat system-of-systems in which it is embedded. Consequently, although the individual platform's performance may be excellent, it struggles to play its intended role in a real system-of-systems confrontation environment, and may even induce "negative emergence" phenomena due to poor coordination among equipment [6].

In recent years, some researchers have begun to introduce the idea of system-of-systems design into the aircraft conceptual design phase. Biltgen proposed an optimization framework that divides the system-of-systems into three levels: "system-of-systems – system – subsystem" [7]; Liu et al. put forward a system-of-systems-oriented aircraft conceptual design process and provided references for the key technologies at each step [8]. The "Effectiveness-Driven Rapid Design of Aircraft Platforms" [9]project carried out by the U.S. Air Force Research Laboratory (AFRL) also reflects this trend. As illustrated in Figure 1, its process starts from underlying performance parameters, generates a conceptual layout through an integration center, sequentially conducts flight, lethality, and stealth performance analyses, and then obtains system-of-systems effectiveness based on simulation scenarios, using the effectiveness value as the criterion for judging the merits of a configuration. Similarly, Dietl et al. conducted research on fighter aircraft design and fleet effectiveness evaluation based on system-of-systems battlespace simulation [10]. This approach enables rapid verification of multiple layout configurations during the conceptual phase, thereby reducing the risk of subsequent design changes. Bi Wenhao et al. further expanded the research boundaries of this field by proposing a system-of-systems architecture design and modeling method based on complex adaptive systems theory for manned/unmanned cooperative air combat scenarios [11]. However, most of these studies still remain at the level of framework exploration and lack practical examples that deeply integrate specific intelligent optimization algorithms with system-of-systems effectiveness simulation. For instance, although the WUADS tool developed by Kiely and Agarwal can achieve rapid conceptual modeling of commercial aircraft, it does not incorporate system-of-systems effectiveness into the closed-loop optimization.

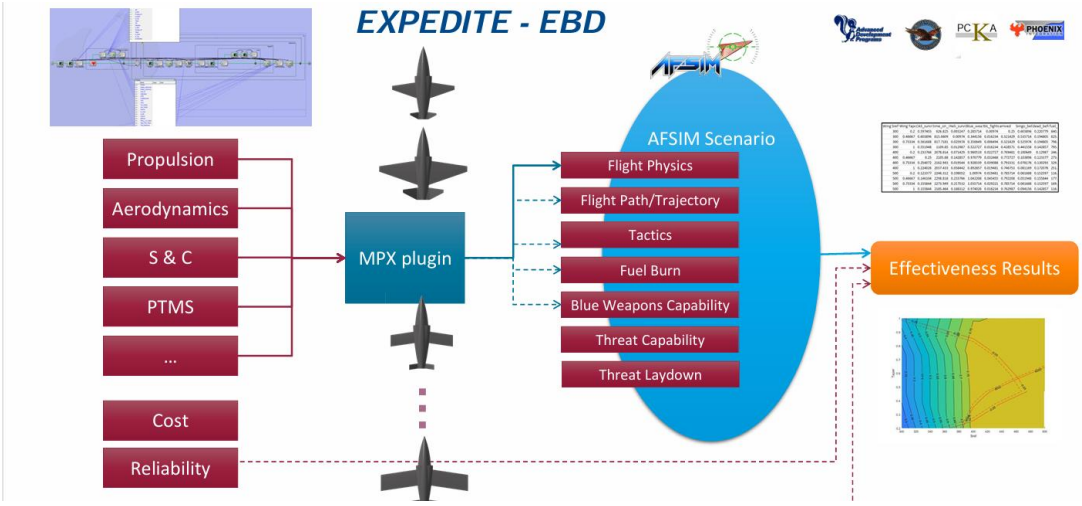


Figure 1 – Effectiveness-driven rapid design of aircraft platforms

To address the above issues, this paper proposes an effectiveness-driven intelligent optimization method for the conceptual layout of air combat equipment. Aiming to maximize the overall effectiveness of the air combat system-of-systems, the method constructs a cross-level optimization framework of "layout parameters – aircraft performance – system-of-systems effectiveness." At the optimization algorithm level, an improved genetic algorithm is adopted as the optimization engine, where the aircraft conceptual layout parameters are real-number encoded. A selection strategy combining elitism preservation and fitness-proportionate selection, a uniform crossover operator, and an adaptive mutation operator are designed, with the system-of-systems effectiveness simulation results serving as the fitness function. At the performance estimation level, engineering empirical formulas for subsonic aircraft design are used to rapidly estimate key flight performance metrics such as cruise speed, fuel capacity, and fuel consumption rate. Meanwhile, the Physical Optics method is employed to calculate the radar cross-section (RCS) of the aircraft in five characteristic directions, and omnidirectional RCS characteristics are obtained through interpolation. At the simulation validation level, based on the Agent-Based Modeling and Simulation (ABMS) concept, an air combat system-of-systems effectiveness simulation platform comprising motion, detection, weapon, and communication modules is constructed [12][13], providing a controllable and repeatable closed-loop experimental environment for the optimization algorithm. The entire method forms a closed-loop process of "design – simulation – optimization," capable of automatically and iteratively searching for aircraft conceptual layout schemes that achieve optimal system-of-systems effectiveness.

2. Effectiveness-Driven Intelligent Optimization Method for Conceptual Layout of Air Combat Equipment

2.1 Overall Optimization Framework

The core idea of the effectiveness-driven intelligent optimization method for aircraft conceptual layout proposed in this paper is to form a closed-loop optimization loop by integrating aircraft platform layout design with air combat system-of-systems effectiveness evaluation through a genetic algorithm, so that the optimization process is directly oriented toward maximizing system-of-systems effectiveness. The overall framework of the method is shown in Figure 2, which consists of three mutually coupled core modules: the parametric modeling and performance estimation module, the air combat system-of-systems effectiveness simulation module, and the improved genetic algorithm module.

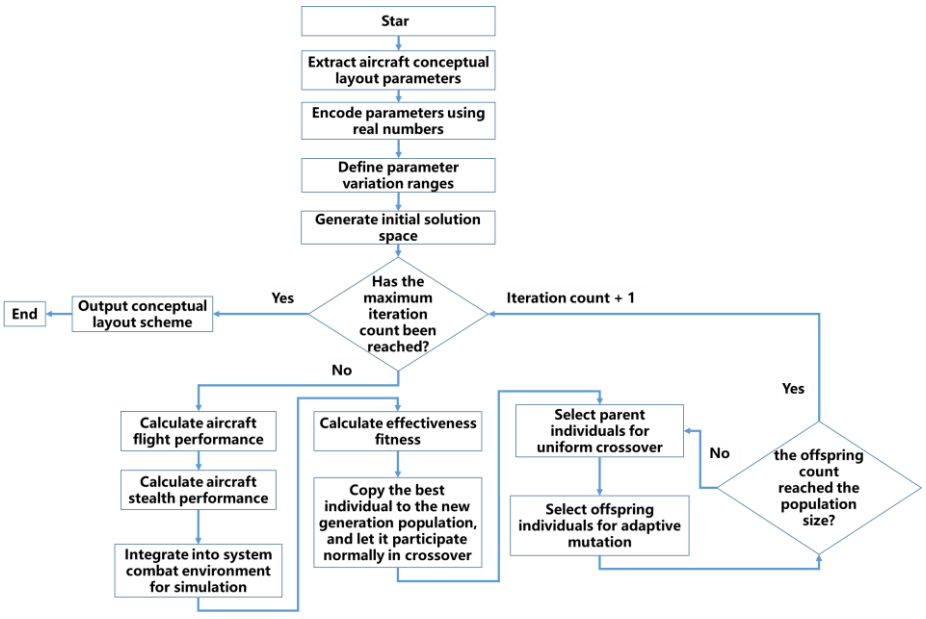


Figure 2 – Implementation framework of an effectiveness-driven intelligent optimization method for aircraft conceptual layout

In each iteration of the optimization, the genetic algorithm first performs real-number encoding on the aircraft's conceptual layout parameters (such as wingspan, chord length, sweep angle, fuselage dimensions, tail area, etc.) to generate an initial population or a new generation of offspring. For each individual in the population (i.e., a specific layout scheme), the performance estimation module is invoked to rapidly calculate its flight performance parameters—including cruise speed, fuel capacity, fuel consumption rate, thrust-to-weight ratio, and wing loading—based on engineering empirical formulas for subsonic aircraft design [14]. Simultaneously, the Physical Optics method is employed to estimate the radar cross-section (RCS) in five characteristic directions, and omnidirectional RCS characteristics are obtained through interpolation. After the performance estimation is completed, the parameters of the layout scheme are loaded into the air combat system-of-systems effectiveness simulation platform [15][16]to drive red-blue confrontation simulations set against typical mission scenarios. The simulation platform comprehensively weighs the degree of damage to friendly and enemy equipment as well as the degree of mission accomplishment, and outputs a system-of-systems effectiveness score, which directly serves as the fitness value of that individual in the genetic algorithm. Subsequently, based on the fitness values of all individuals in the population, the genetic algorithm adopts a selection strategy that combines elitism preservation and fitness-proportionate selection to select parent individuals, generates a new generation population through uniform crossover and adaptive mutation operations, and proceeds to the next iteration. The above process is executed iteratively until the convergence condition is met or the preset maximum number of iterations is reached, ultimately outputting the aircraft conceptual layout scheme that achieves optimal air combat system-of-systems effectiveness.

2.2 Aircraft Conceptual Layout Performance Estimation

In the aircraft conceptual layout design phase, the rapid estimation of aerodynamic and stealth performance is critical for closed-loop optimization iterations. Based on the input requirements of the system-of-systems effectiveness simulation, this paper selects the performance parameters most closely associated with the aircraft platform constraints for modeling. The extracted geometric parameters of the conceptual layout are defined as shown in Table 1. These parameters directly determine the lift-to-drag characteristics, stability, and radar detectability of the aircraft. This paper does not consider the detailed modeling of structures and control systems, but focuses solely on the rapid generation of flight performance and omnidirectional radar stealth characteristics to drive the subsequent effectiveness simulation.

Table 1 Conceptual layout parameters

Layout Parameter	Definition
Wingspan (b)	The span length of the aircraft wing, i.e., the distance from wingtip to wingtip
Wing Root Chord (c_0)	The width of the wing at the root
Wing Tip Chord (c_1)	The width of the wing at the tip
Wing Leading-Edge Sweep Angle (α_1)	The angle between the wing leading edge and the fuselage centerline
Fuselage Radius (r)	Fuselage cross-sectional area
Fuselage Length (L)	The distance from the nose to the tail
Vertical Tail Area (S_V)	The area of the vertical tail
Horizontal Tail Area (S_H)	The area of the horizontal tail

1) Geometric Characteristics and Weight Estimation [17]

The wing area is the reference area enclosed by extending the leading and trailing edges of the wing to the aircraft centerline, and its estimation formula is shown in Equation (1).

$$S = \frac{b}{2}\left(c_0 + c_1\right) \tag{1}$$

Where: c_0 is the wing root chord; c_1 is the wing tip chord; b is the wingspan.

The exposed wing planform area is the wing's top-view projected area, and its calculation formula is shown in Equation (2).

$$S_\exp osed = \left(\frac{b}{2} - r\right) \cdot \left(c_0 + c_1\right) \tag{2}$$

Where: c_0 is the wing root chord; c_1 is the wing tip chord; b is the wingspan; r is the fuselage radius.

The fuselage wetted area can be estimated from the aircraft's side-view projected area and top-view projected area, and its calculation formula is shown in Equation (3).

$$S_WET1 = \mathrm{K}\left(\frac{A_side + A_top}{2}\right) \tag{3}$$

Where: A_side is the side-view projected area; A_top is the top-view projected area; $K=\pi$ when the fuselage cross-section is circular and the fuselage is slender; $K=4$ when the fuselage cross-section is rectangular; $K=3.4$ for a fuselage with a general cross-sectional shape.

The wetted area of the wing and tail surfaces can be estimated based on their planform shapes. The wetted area is obtained by multiplying the exposed planform area in the actual view by an approximation factor, and its calculation formula is shown in Equation (4).

$$S_WET2 = 2.003 S_exposed \tag{4}$$

Where: $S_exposed$ is the exposed planform area of the wing.

The aircraft empty weight is typically estimated using the approximate classified weight method based on typical values. The weight of the wing and tail surfaces is determined by the weight per unit exposed area of existing aircraft; the fuselage weight is determined according to the wetted area of the fuselage; the landing gear weight is estimated as a percentage of the takeoff weight; the installed engine weight is obtained by multiplying the engine weight by a coefficient; and all the remaining items that belong to the empty weight category can also be estimated as a percentage fraction of the takeoff weight. Therefore, the estimation formula for the aircraft empty weight is shown in Equation (5).

$$M_E = \frac{\left(A1 \cdot S_exposed + A2 \cdot S_V + A3 \cdot S_H + A4 \cdot S_WET1 + A5 \cdot M_fa\right)}{0.8} \tag{5}$$

Where: $A1$ is the wing multiplication coefficient; $A2$ is the vertical tail multiplication coefficient; $A3$ is the horizontal tail multiplication coefficient; $A4$ is the fuselage multiplication coefficient; $A5$ is the engine multiplication coefficient; $S_exposed$ is the wing exposed planform area; S_V is the vertical tail area; S_H is the horizontal tail area; S_WET1 is the fuselage wetted area; M_fa is the engine weight.

The total aircraft weight can be estimated from the empty weight using an empirical formula, as shown in Equation (6).

$$\frac{M}{M_E} = A\left(M_E^{C}\right) K_{VS} \tag{6}$$

Where: M is the total takeoff weight; M_E is the empty weight; A is a multiplication coefficient; C is a multiplication coefficient; K_{VS} is the variable-sweep constant, which is taken as 1.04 for variable-sweep wings and 1 for fixed-sweep wings.

The fuel weight estimation formula is shown in Equation (7).

$$M_F = M - M_E - M_PL - M_crew \tag{7}$$

Where: M_F is the fuel weight; M is the takeoff weight; M_E is the empty weight; M_PL is the payload weight; M_crew is the crew weight.

2) Aerodynamic Characteristics and Flight Performance Estimation

The calculation formula for the cosine of the wing quarter-chord sweep angle is shown in Equation (8).

$$\cos(a_2) = \frac{(3c_0 + c_1)}{2(c_0 + c_1)} \cdot \cos(a_1) \tag{8}$$

Where: $\cos(a_2)$ is the cosine of the wing quarter-chord sweep angle; c_0 is the wing root chord; c_1 is the wing tip chord; a_1 is the wing leading-edge sweep angle.

The estimation formula for the wing maximum lift coefficient is shown in Equation (9).

$$C_{LMAX} = 0.9 c_{lmax} \cdot \cos(a_2) \tag{9}$$

Where: C_{LMAX} is the wing maximum lift coefficient; c_{lmax} is the maximum lift coefficient of an unswept wing; $\cos(a_2)$ is the cosine of the wing quarter-chord sweep angle.

The estimation formula for the aircraft cruise speed is shown in Equation (10).

$$v = \sqrt{\frac{2Mg}{0.8 S \rho C_{LMAX}}} \tag{10}$$

Where: v is the aircraft cruise speed; $M \times g$ is the aircraft takeoff weight; C_{LMAX} is the wing maximum lift coefficient; ρ is the atmospheric density; S is the wing area.

The calculation formula for the aspect ratio is shown in Equation (11).

$$A = \frac{b^2}{S} \tag{11}$$

Where: A is the wing aspect ratio; b is the wingspan; S is the wing area.

The estimation formula for the fuselage lift factor is shown in Equation (12).

$$F = 1.07(1 + \frac{r}{b})^2 \tag{12}$$

Where: F is the fuselage lift factor; r is the fuselage radius; b is the wingspan.

The semi-empirical formula for the lift-curve slope of a complete subsonic wing is shown in Equation (13).

$$C_{L\alpha} = \frac{\left(\frac{\pi}{180} \cdot (2 \cdot \pi \cdot A) \cdot \frac{S_exposed}{S}\right) \cdot F}{2 + \left(4 + \left(A^2 \cdot \left(1 - Ma^2\right) / 0.9^2\right) \cdot \left(1 + \tan(a_1)^2 / \left(1 - Ma^2\right)\right)^{0.5}\right.} \tag{13}$$

Where: $C_{L\alpha}$ is the lift-curve slope of a complete subsonic wing; A is the aspect ratio; $S_exposed$ is the wing exposed planform area; S is the wing area; F is the fuselage lift factor; Ma is the aircraft flight Mach number; a_1 is the wing leading-edge sweep angle.

The estimation formula for the aircraft angle of attack (relative to the zero-lift angle of attack) is shown in Equation (14).

$$\alpha = \frac{0.8C_{LMAX}}{C_{L\alpha}} \tag{14}$$

Where : α is the angle of attack; C_{LMAX} is the wing maximum lift coefficient; $C_{L\alpha}$ is the lift-curve slope of a complete subsonic wing.

The aircraft drag consists of two components, and its calculation formula is shown in Equation (15).

$$C_D = C_{D0} + K_1(0.8C_{LMAX})^2 \tag{15}$$

Where: C_D is the total aircraft drag coefficient; C_{D0} is the zero-lift drag coefficient; K_1 is the lift-induced drag factor; C_{LMAX} is the wing maximum lift coefficient.

This paper adopts the equivalent skin-friction method and the component buildup method for estimating the zero-lift drag characteristics. The estimation formula for the subsonic zero-lift drag coefficient of the entire aircraft is shown in Equation (16).

$$C_{D0} = c_{fe} \cdot \frac{S_WET1 + S_WET2}{S} \tag{16}$$

Where: C_{D0} is the zero-lift drag coefficient; c_{fe} is the equivalent skin friction drag coefficient; S_WET1 is the fuselage wetted area; S_WET2 is the wetted area of the wing and tail surfaces; S is the wing area.

The estimation formula for the lift-induced drag factor of a subsonic swept-wing aircraft is shown in Equations (17) and (18).

$$K_1 = \frac{1}{\pi Ae} \tag{17}$$

$$e = (4.61\left(1 - 0.045 \cdot A^{0.68}\right)\cos(a_1)^{0.15}) - 3.1 \tag{18}$$

Where: A is the wing area; e is the Oswald efficiency factor; a_1 is the wing leading-edge sweep angle.

Under cruise conditions, the equilibrium equation indicates that the aircraft drag equals the thrust. Hence, the estimation formulas for the total aircraft drag, thrust, and fuel consumption rate are shown in Equations (19), (20), (21), and (22).

$$D_0 = \frac{1}{2}\rho v^2 (S_WET1 + S_WET2)C_{D0} \tag{19}$$

$$D = \frac{1}{2}\rho v^2 SK_1(0.8C_{LMAX})^2 \tag{20}$$

$$\mathrm{T} = \mathrm{D}_0 + \mathrm{D} \tag{21}$$

$$consumption_rate = \frac{T}{gI_{sp}} \tag{22}$$

Where: D_0 is the zero-lift drag; ρ is the atmospheric density; v is the aircraft cruise speed; S_WET1 is the fuselage wetted area; S_WET2 is the wetted area of the wing and tail surfaces; C_{D0} is the zero-lift drag coefficient; D is the lift-induced drag; S is the wing area; K_1 is the lift-induced drag factor; C_{LMAX} is the wing maximum lift coefficient; T is the required thrust of the aircraft; $consumption_rate$ is the fuel consumption rate; I_{sp} is the engine specific impulse.

To ensure the engineering feasibility of the generated layout, the thrust-to-weight ratio is introduced

as a constraint filter. If the thrust-to-weight ratio or wing loading of a layout exceeds the typical range of the corresponding aircraft type (e.g., the takeoff thrust-to-weight ratio of a jet fighter is approximately 0.6–0.9, and the wing loading is approximately 342 kg/m²), an extremely low fitness value is directly assigned to prevent invalid individuals from entering subsequent genetic operations.

3) Stealth Performance Estimation

For the rapid estimation of radar cross section (RCS) during the conceptual layout phase, this paper adopts the Physical Optics method [18][19]. Given the local behavior of electromagnetic scattering in the high-frequency region, the induced surface current on the target is expressed as shown in Equation (23).

$$J_S = 2\vec{n} \times H_{\mathrm{i}} \tag{23}$$

Where: J_S is the surface current; $\vec{n}$ is the surface outward normal vector; H_{i} is the magnetic field intensity at the incident point.

The surface current value calculated by this method is not an exact solution, but rather an approximate one. The accuracy of this approximation is closely related to the geometric characteristics of the scatterer. When the scatterer surface can be approximated as planar in the vicinity of the incident point—that is, when the radius of curvature of the object surface is much larger than the electromagnetic wavelength—the deviation between the approximate solution and the actual value is small.

The definition of RCS is based on the assumption of a point target illuminated by a plane wave, and its mathematical expression is shown in Equation (24).

$$\sigma = \lim_{R\to\infty} 4\pi R^2 \left| \frac{E_{\mathrm{s}}}{E_{\mathrm{i}}} \right| \tag{24}$$

Where: E_{i} is the incident electric field intensity; E_{s} is the surface outward normal vector; R is the distance from the target to the radar.

When the polarization of the receiving antenna and the phase factor are taken into account, the RCS can be expressed as shown in Equation (25).

$$\sqrt{\sigma} = \lim_{R\to\infty} \sqrt{4\pi R^2}\, \frac{\vec{e_s} E_{\mathrm{s}}}{|E_{\mathrm{i}}|} \tag{25}$$

Where: $\vec{e_s}$ is the incident electric field intensity.

When the field point r' and the source point r are far apart, the Green's function simplifies to the far-field Green's function, as shown in Equation (26).

$$G \approx \frac{e^{-jkr}}{4\pi r} \tag{26}$$

In the far-field region, the gradient operator can be replaced by $-jk\vec{s}$, and therefore the far-field electric field calculation formula is given by Equation (27).

$$E_{\mathrm{s}} = \frac{e^{-jkr}}{4\pi r}(-j\omega\mu)\int_S J_S e^{-jk\vec{s}\cdot r} dS + jk\vec{s}\,\frac{1}{\varepsilon}\int_S \rho_S e^{jk\vec{s}\cdot r} dS \tag{27}$$

Considering $\vec{e_s}\cdot\vec{s} = 0$, the RCS calculation formula is shown in Equation (28).

$$\sqrt{\sigma} = \sqrt{4\pi R^2}\,\frac{1}{|E_{\mathrm{i}}|}\left(-j\omega\mu \frac{e^{-jkr}}{4\pi r}\int_S \vec{e_S}\cdot J_S e^{jk\vec{s}\cdot r} dS \right) \tag{28}$$

Substituting the surface current calculation formula yields:

$$\sqrt{\sigma}=\sqrt{4\pi R^2}\frac{1}{|E_{\mathrm{i}}|}\left(-j\omega\mu\frac{e^{-jkr}}{4\pi r}2\int_S\overrightarrow{e_S}\cdot\left(\vec{n}\times H_{\mathrm{i}}\right)e^{jk\vec{s}\cdot r}dS\right) \tag{29}$$

Based on the relationship between the electric and magnetic fields, we have $E_{\mathrm{i}}=\eta H_{\mathrm{i}}$, and combined with $\omega\mu=k\eta$, the expression for RCS is obtained as:

$$\sqrt{\sigma}=\frac{jk}{\sqrt{\pi}}\vec{n}\cdot\left(\overrightarrow{e_S}\times\overrightarrow{h_i}\right)\int_S e^{jkw\cdot r}dS \tag{30}$$

Solving the integral yields the RCS value at normal incidence as:

$$\sqrt{\sigma}=\frac{jk}{\sqrt{\pi}}\vec{n}\cdot\left(\overrightarrow{e_S}\times\overrightarrow{h_i}\right)e^{jkw\cdot r}A \tag{31}$$

At this point, the RCS values in the five directions—front, rear, top, bottom, and side—of the aircraft can be estimated using the Physical Optics method. Based on these RCS values at these angles, the omnidirectional radar signature values can then be obtained using the interpolation formula [20]. The definition of the aircraft's azimuth and elevation angles is shown in Figure 3.

$$\sigma_{(\varphi,\phi)}=\sigma_1(1-\sqrt{|\sin\phi|})(1-\sqrt{|\sin\varphi|})+\sigma_2|\sin\phi|+\sigma_3(1-\sqrt{|\sin\phi|})|\sin\varphi|$$

$$\begin{cases}\sigma_1=\begin{cases}\sigma_x & (-90<\varphi<90)\\ \sigma_{-x} & (-180<\varphi<-90\cup 90<\varphi<180)\end{cases}\\ \sigma_2=\begin{cases}\sigma_z & (\phi\geq 0)\\ \sigma_{-z} & (\phi<0)\end{cases}\\ \sigma_3=\sigma_y\end{cases} \tag{32}$$

Where: ϕ is the detection elevation angle, positive when observed from above the aircraft; φ is the detection azimuth angle, positive when observed from the right side of the aircraft nose.

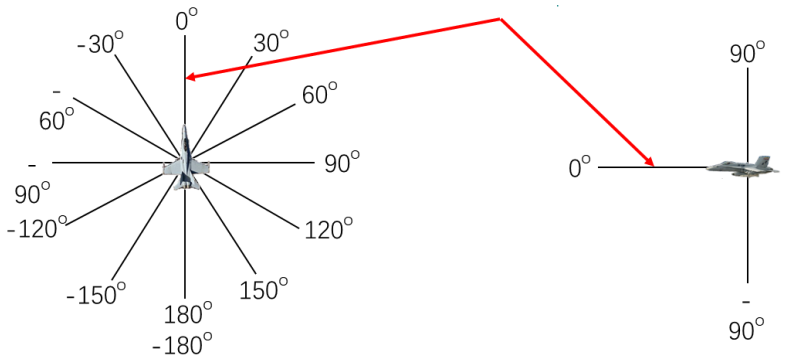


Figure 3 – Elevation and azimuth angle convention

2.3 Parameter Encoding, Operator Selection, and Effectiveness Fitness Function Design

In the implementation of the genetic algorithm, the encoding method directly affects search efficiency and solution quality. Since the variation of aircraft conceptual layout parameters is continuous and smooth, this paper adopts real-number encoding to represent individuals in the solution space. This encoding approach avoids the precision loss problem caused by binary encoding and is more suitable for solving continuous optimization problems. Defining a chromosome as a complete layout scheme and genes as corresponding specific layout parameters, the aircraft conceptual layout can be expressed as:

$$A=\{a_1 \quad a_2 \quad a_3 \quad a_4 \quad a_5 \quad a_6 \quad a_7 \quad a_8\}=\{b \quad c_0 \quad c_1 \quad a_1 \quad r \quad L \quad S_V \quad S_H\} \tag{33}$$

The role of the selection operator is to select superior individuals from the current population as parents to produce the next generation. To ensure algorithm convergence while maintaining population diversity, this paper adopts a method that combines elitism preservation with fitness-proportionate selection. The elitism preservation strategy directly copies the individual with the highest fitness in the current population into the next generation population, ensuring that the optimal solution is not lost due to subsequent crossover and mutation operations. Fitness-proportionate selection determines the probability of an individual being selected based on the proportion of its fitness to the total fitness of the population; individuals with higher fitness have a greater chance of being selected as parents. The combined use of these two strategies not only ensures the stability of the best individual's effectiveness in the population but also ensures that superior individuals have the opportunity to be selected as parents, thereby improving the convergence speed of the algorithm.

The crossover operator is responsible for recombining the genes of two parent individuals to generate offspring. Among various crossover strategies, the uniform crossover operator is favored for its unique characteristics. For any two paired parent individuals, each gene locus on their encoding strings is exchanged with the same probability. This exchange mechanism does not depend on the position of the gene locus in the encoding string, nor does it consider the interrelationships between genes, thereby ensuring the randomness and uniformity of gene exchange. In this way, the uniform crossover operator can promote a uniform distribution of genes within the population, helping the algorithm explore a broader solution space during the search process while reducing the risk of premature convergence to a local optimum.

The mutation operator introduces new genetic information by randomly perturbing certain gene loci in an individual [21], which plays a critical role in maintaining population diversity and preventing the algorithm from falling into local optima. In this paper, an adaptive uniform mutation operator is designed, whose core idea is to dynamically adjust the mutation probability of each gene locus according to the average fitness of the population. The calculation formula for the mutation probability is as follows:

$$prob=(actual_target_y-average_fitness)\cdot 0.2+0.1 \tag{34}$$

Where: $prob$ is the mutation probability; $actual_target_y$ is the target fitness; $average_fitness$ is the population average fitness.

From this formula, it can be seen that when the population average fitness is low, individual differences are large, and the population has not yet converged, the mutation probability takes a relatively high value, which facilitates global exploration and helps avoid falling into local optima. As the population average fitness gradually approaches the maximum fitness, i.e., as the population tends to converge, the mutation probability automatically decreases, thereby reducing the risk of superior individuals degenerating into inferior ones due to mutation. This adaptive mechanism effectively balances the contradiction between exploration and exploitation in the search process.

The fitness function is the core criterion for evaluating the quality of individuals in a genetic algorithm and the sole driving force behind the algorithm's evolution. In this paper, the fitness of an individual is defined as the system-of-systems effectiveness value achieved by the aircraft conceptual layout it represents in the air combat system-of-systems effectiveness simulation. Specifically, after the flight performance and stealth performance estimations are completed, the aircraft model is deployed into the Agent-based air combat confrontation simulation platform, a full combat scenario simulation is run, and the engagement results are recorded. The calculation of the system-of-systems effectiveness value comprehensively considers the damage to friendly equipment, the damage to enemy equipment, and the degree of mission completion. Let the importance weight vector of the blue-side (friendly) equipment be w_{blue}, and that of the red-side (enemy) equipment be w_{red}. During the simulation, if a piece of blue-side equipment is destroyed, a negative value $-w_{blue,l}$ is recorded; if a piece of red-side equipment is destroyed, a positive value $+w_{red}$ is recorded. All recorded values

are summed and then adjusted according to the mission completion status (e.g., whether the key target has been destroyed), yielding the system-of-systems effectiveness fitness score F for that simulation. The specific definition of the fitness function will be further elaborated in the case study in Section 4. Through this approach, the fitness function directly links the underlying layout parameters with the top-level system-of-systems effectiveness, guiding the genetic algorithm to search for the optimal layout scheme in a direction that maximizes system-of-systems effectiveness.

3. Case Verification

3.1 Typical Combat Scenario and Simulation Environment

To validate the effectiveness of the proposed method, this section constructs a typical air combat system-of-systems confrontation scenario, set against the background of fighters escorting a bomber to carry out an air-to-surface strike mission, where the red and blue sides confront each other over the destruction and defense of critical ground targets. The scenario configuration is shown in Figure 4. The blue-side combat formation includes: one early warning aircraft, responsible for searching the engagement area and obtaining rough position information of red-side targets; one bomber, serving as the optimization object and also acting as the formation command node, which receives precise target information relayed back by fighters and launches air-to-surface missiles to destroy critical red-side targets [22]; and four fighters, performing tasks such as escorting, intercepting red-side interceptors, and transmitting precise target locations. The red side deploys six fighters, evenly distributed around the critical targets, tasked with intercepting the intruding blue-side formation. The performance parameters of the fighters on both the red and blue sides remain identical.

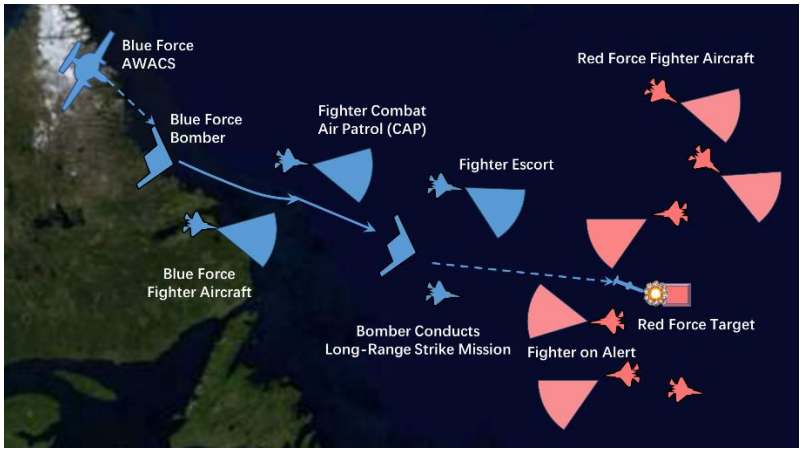


Figure 4 – Schematic of the air combat engagement scenario

Taking the blue-side integrated combat system-of-systems as the research object, its main operational process is as follows: The blue-side early warning aircraft conducts reconnaissance in front of the enemy, obtains the approximate location information of red-side targets, and guides the fighters and bomber to advance and execute the mission, continuously providing information support to the combat system-of-systems. In the subsequent attack mission, the bomber serves as the overall commander, and Fighter A serves as the deputy commander, responsible for the position dispatch of the fighter group. When encountering a threat, Fighter A dispatches the remaining fighters to carry out interception; after completing the interception mission, each aircraft automatically returns to the formation to continue escorting. If Fighter 1 is destroyed, Fighter 2 takes over as the deputy commander and continues to command the operation [23]. The bomber maintains a silent state and does not conduct radar detection; once the fighters detect the precise position information of red-side targets, they transmit it to the bomber, which then makes its own decisions based on the battlefield situational information of the air-to-surface missiles and carries out the air-to-surface strike. In addition, the three fighters numbered 2, 3, and 4 in the fighter formation also carry air-to-surface missiles and can launch attacks against enemy targets, but with lower lethality effectiveness. The

red-blue system-of-systems confrontation simulation platform is shown in Figure 5.

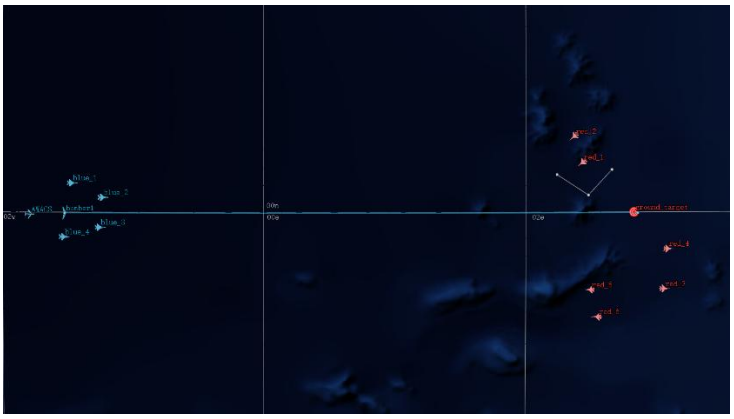


Figure 5 – Red-blue simulation scenario

During the mission, the early warning aircraft is responsible for searching the engagement area and providing approximate location information of the mission targets, while the bomber and fighters form a formation to advance and execute the mission. Throughout the engagement, the bomber remains in a silent state at all times; after receiving the precise target location information relayed back by the fighters, it launches two air-to-surface missiles to carry out the strike. The fighters provide escort throughout the entire process. Upon encountering enemy intercepting fighters, they proactively engage to protect their own bomber, and after completing the interception, they automatically return to the flanks of the bomber and remain on alert, as shown in Figures 6 and 7.

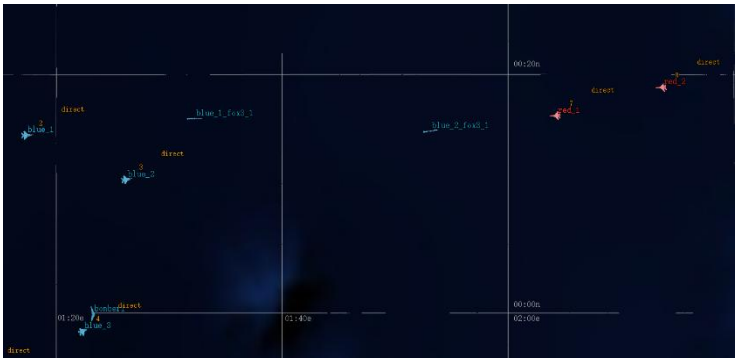


Figure 6 – Fighters advancing to intercept enemy threats

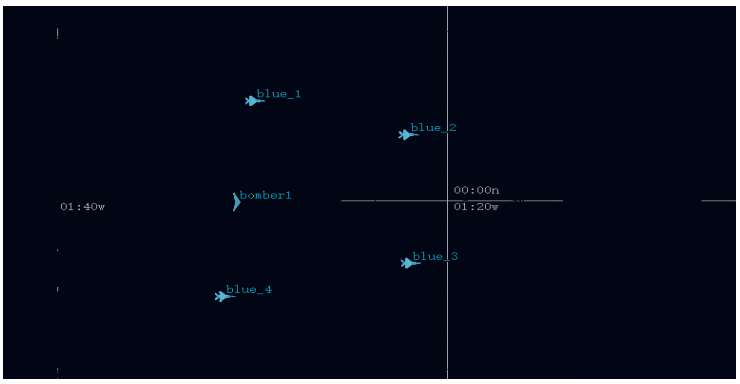


Figure 7 –Fighters escorting

In this mission scenario, the fighters of both the red and blue sides have identical performance. From a static perspective, if all six red-side fighters were committed to battle, they could essentially

annihilate the four blue-side fighters and the bomber. However, from a dynamic perspective, the blue-side fighters can engage almost simultaneously, whereas the red-side fighters are distributed around the target point and cannot all reach the front line at the same time in the first instance, which creates a possibility for the blue side to accomplish its mission. Under these circumstances, stealth capability becomes particularly important. If the enemy can be engaged at a position closer to the target point, it can create more attack opportunities for the bomber, delay the assembly of the red-side fighters, and buy more time for the formation to withdraw. At the same time, fuel capacity, fuel consumption rate, and flight speed determine the mission range satisfaction of the bomber, and since it may face interception and pursuit by red-side fighters, the bomber's flight performance will also greatly affect the overall maneuverability of the formation. Therefore, it is necessary to carry out a genetic algorithm-based conceptual layout optimization design for the bomber, so that the flight performance and stealth performance of the aircraft can match the air combat system-of-systems to the greatest extent, thereby maximizing the system-of-systems operational effectiveness.

3.2 Fitness Function and Algorithm Design

Based on the idea of effectiveness-driven optimization design, this section designs an effectiveness fitness function oriented toward the air combat system-of-systems confrontation scenario. The importance weight vector of the blue-side equipment is stipulated as $\boldsymbol{w}^1 = (0.05,\ 0.05,\ 0.05,\ 0.05,\ 0.8)$, and that of the red-side equipment as $\boldsymbol{w}^2 = (0.05,\ 0.05,\ 0.05,\ 0.05,\ 0.05,\ 0.05,\ 0.7)$. During the simulation, if a piece of blue-side equipment is destroyed, a negative value of its equipment importance weight $-w_i^1$ is recorded; if a piece of red-side equipment is destroyed, a positive value of its equipment importance weight w_i^2 is recorded. All recorded values are summed, and the resulting sum is the air combat system-of-systems effectiveness fitness score in that state. On this basis, the target fitness value is set to 1, and the effectiveness fitness function in the algorithm is thus constructed, as shown in Equation (35).

$$F = 1 - \left(w2_i - w1_i \right) \tag{35}$$

The pseudocode of the effectiveness-driven intelligent optimization algorithm for aircraft conceptual layout thus designed is shown in Table 2.

Table 2 Pseudocode of the effectiveness-driven intelligent optimization algorithm for aircraft conceptual layout

Algorithm Effectiveness-Driven Intelligent Optimization Algorithm for Aircraft Conceptual Layout
Input: Conceptual layout parameter combination, population size population_size, number of iterations num_generations
Output: Optimal conceptual layout parameter combination space
1: Initialize a population of key equipment conceptual layout parameter combination spaces with the size of population_size
2: Loop (for each generation):
3: Loop (for each individual):
4: Calculate the individual's flight performance and stealth performance
5: Preliminarily verify whether the equipment conceptual layout's thrust-to-weight ratio and wing loading fall within the specified range; if not, directly assign an effectiveness value of -1
6: Write the filtered individual's performance parameters into the simulation file
7: Start the simulation program
8: Wait for the simulation to finish and read the results
9: Add the results to column_sums
10: Calculate the system-of-systems fitness score F at this time

11: Find the best individual best_individual and its fitness score, and directly copy it into the new population
12: Screen individuals in the population using an operator combining elitism preservation and fitness-proportionate selection
13: Perform crossover inheritance on the selected individuals using a uniform crossover operator
14: Perform mutation operations on the newly generated individuals using an adaptive mutation operator
15: Add the offspring to the new population new_population
16: If the new population size is insufficient, continue crossover and mutation until it reaches population_size
17: Update population to the new population new_population
18: Plot the chart of best fitness score and population average fitness score
19: Return best_individual and best_fitness_scores
20: Until generation = num_generations
21: Return the optimal conceptual layout parameter combination space

3.3 Optimization Results and Analysis

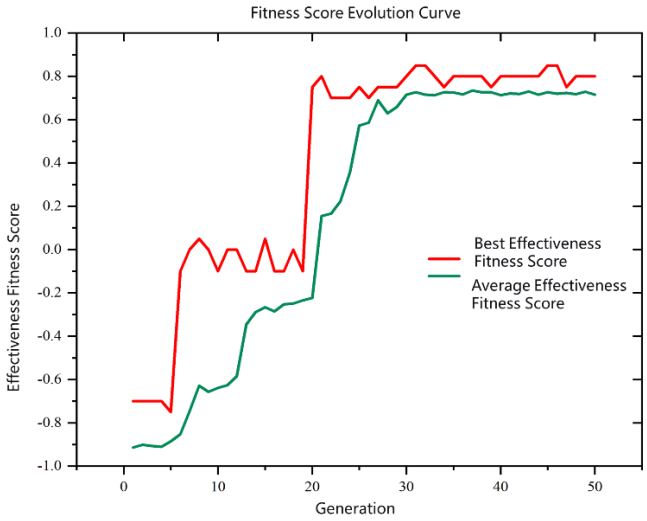


Figure 8 – Fitness score evolution curve under adaptive mutation probability

Figure 8 shows the variation curve of the population's best fitness over iterations under the adaptive mutation probability. As can be seen from the figure, when the population average fitness score is low, the individual mutation probability is high, which ensures optimization efficiency and prevents falling into local optima. When the population average fitness score is high, the individual mutation probability is low, reducing the risk of superior individuals degenerating into inferior ones due to mutation. At the 6th generation, the best individual fitness score is approximately −0.1; by the 20th generation, the best individual fitness score reaches approximately 0.7. Thereafter, the best fitness score gradually converges to 0.8. The population average fitness score also increases with the improvement of the best individual fitness and ultimately tends toward the best fitness score, yielding the optimal conceptual layout scheme.

During the 50-generation iteration process, the conceptual layout of the bomber underwent significant evolution. Figure 9 shows the representative morphological changes of the layout from the initial generation to the final generation.

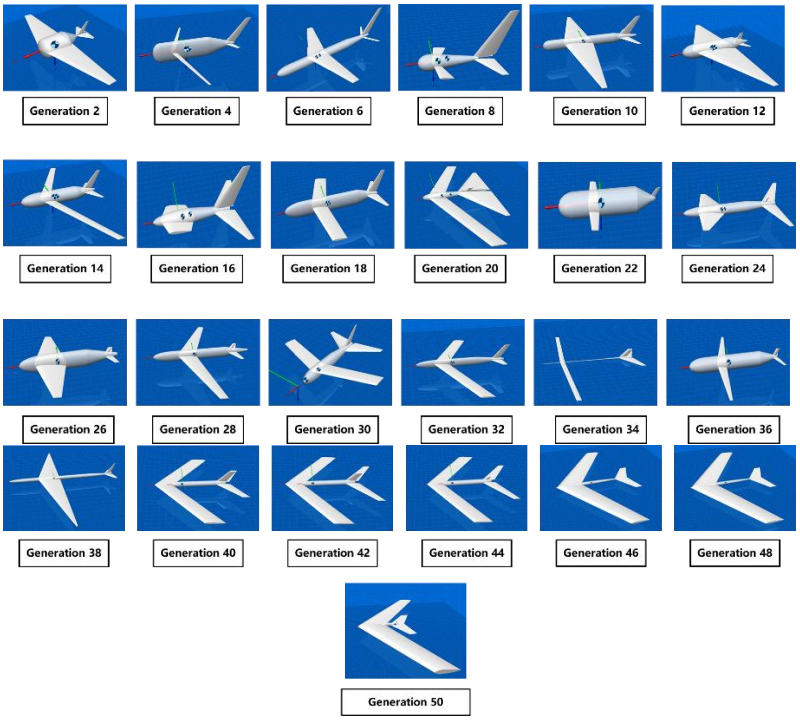


Figure 9 – Conceptual layout diagrams of the optimization process

When the population evolved to the second generation, the conceptual layout and radar signature visualization of the individual with the highest effectiveness value in the population are shown in Figures 10. Its conceptual layout parameters and performance parameters are presented in Table 3.

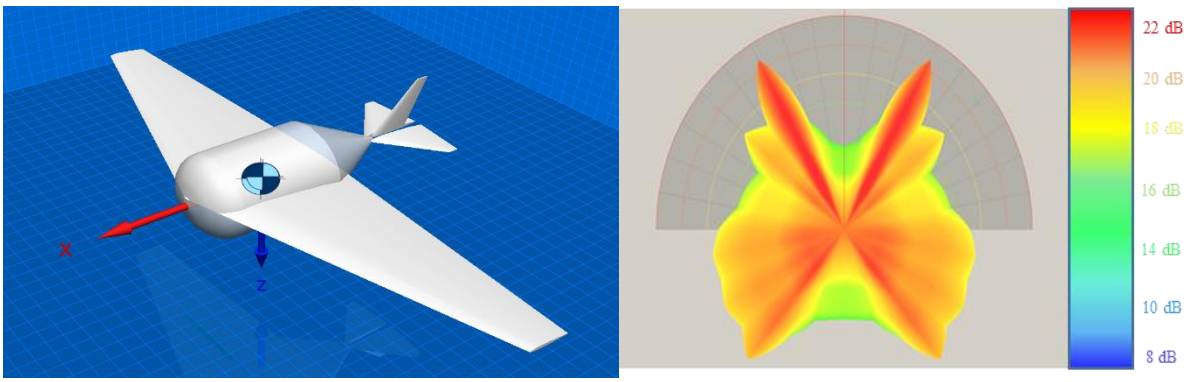


Figure 10 – Second generation conceptual layout and radar signature visualization

Table 3 Conceptual layout and performance parameters

Layout Parameter	Value	Performance and Effectiveness Fitness Data	Value
Wingspan (b)	98.12 (m)	Thrust-to-weight ratio	0.19
Wing Root Chord (c_0)	24.28 (m)	Wing loading	470.08 (kg/m²)
Wing Tip Chord (c_1)	6.54 (m)	Cruise speed	74.46 (m/s)
Wing Leading-Edge Sweep Angle (α_1)	17 (deg)	Fuel capacity	436784.8 (kg)
Fuselage Radius (r)	31.40 (m)	Fuel consumption rate	110.26 (kg/s)
Fuselage Length (L)	33.37 (m)	Effectiveness fitness score	-0.8
Vertical Tail Area (S_V)	40.72 (m²)		
Horizontal Tail Area (S_H)	48.73 (m²)		

The simulation results showed that all friendly fighters and the bomber were destroyed, four enemy fighters were destroyed, and the bomber failed to inflict damage on the enemy target point. From the perspective of flight performance, the large wingspan, large fuselage radius, and large vertical and horizontal tail areas, while contributing to increased lift, also resulted in greater total aircraft drag and a smaller thrust-to-weight ratio. In addition, the larger wing area reduced wing loading but led to an increased fuel consumption rate and decreased cruise speed, resulting in overall poor aircraft maneuverability. From the perspective of stealth performance, the large vertical tail and large fuselage radius caused a significant increase in the aircraft's lateral RCS, resulting in the near-complete loss of stealth capability, leading to premature detection and interception by the enemy.

When the population evolved to the sixth generation, the conceptual layout and radar signature visualization of the individual with the highest effectiveness value in the population are shown in Figures 11. Its conceptual layout parameters and performance parameters are presented in Table 4.

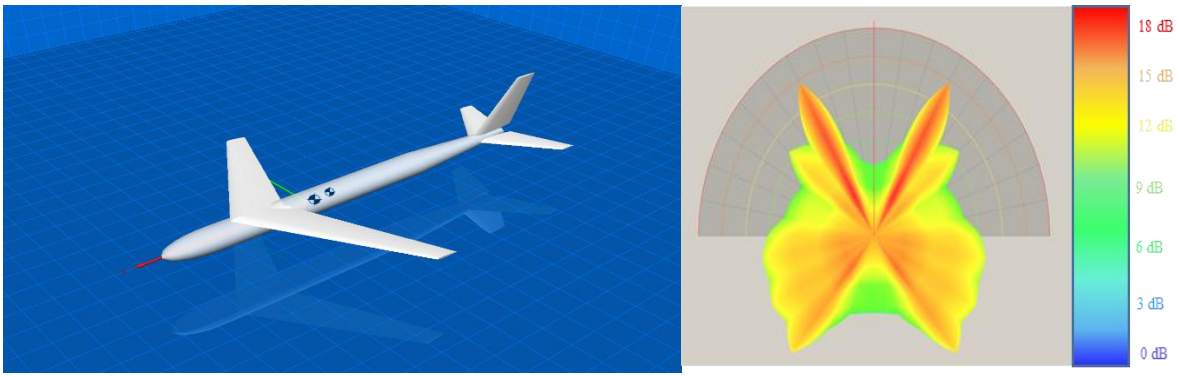


Figure 11 – Sixth generation conceptual layout and radar signature visualization

Table 4 Conceptual layout and performance parameters

Layout Parameter	Value	Performance and Effectiveness Fitness Data	Value
Wingspan (b)	28.38(m)	Thrust-to-weight ratio	0.24
Wing Root Chord (c_0)	5.49(m)	Wing loading	623(kg/m^2)
Wing Tip Chord (c_1)	2.19(m)	Cruise speed	216.82(m/s)
Wing Leading-Edge Sweep Angle (α_1)	33.5(deg)	Fuel capacity	74242.48(kg)
Fuselage Radius (r)	5.02(m)	Fuel consumption rate	7.83(kg/s)
Fuselage Length (L)	39.89(m)	Effectiveness fitness score	-0.1
Vertical Tail Area (S_V)	32.38(m^2)		
Horizontal Tail Area (S_H)	19.24(m^2)		

The simulation results of this generation showed that four enemy fighters were destroyed, while all friendly fighters and the bomber were lost, but the bomber successfully damaged the enemy target. From the perspective of flight performance, compared with the previous generation aircraft, the cruise speed of this generation aircraft was significantly improved, basically meeting the overall maneuverability requirements of the formation. However, due to the reduction in wing area, the wing loading increased correspondingly. From the perspective of stealth performance, the reduction in fuselage radius and vertical tail area reduced the radar signature of the aircraft to some extent, but the effect was not yet significant, and the aircraft still did not achieve a stealthy configuration. Nevertheless, thanks to the increased flight speed and enhanced maneuverability, the bomber was able to complete the strike mission before all the enemy fighters could assemble. However, due to the high weight of the bomber, the calculated system-of-systems fitness score remained relatively low.

When the population evolved to the twentieth generation, the conceptual layout and radar signature visualization of the individual with the highest effectiveness value in the population are shown in Figures 12. Its conceptual layout parameters and performance parameters are presented in Table 5.

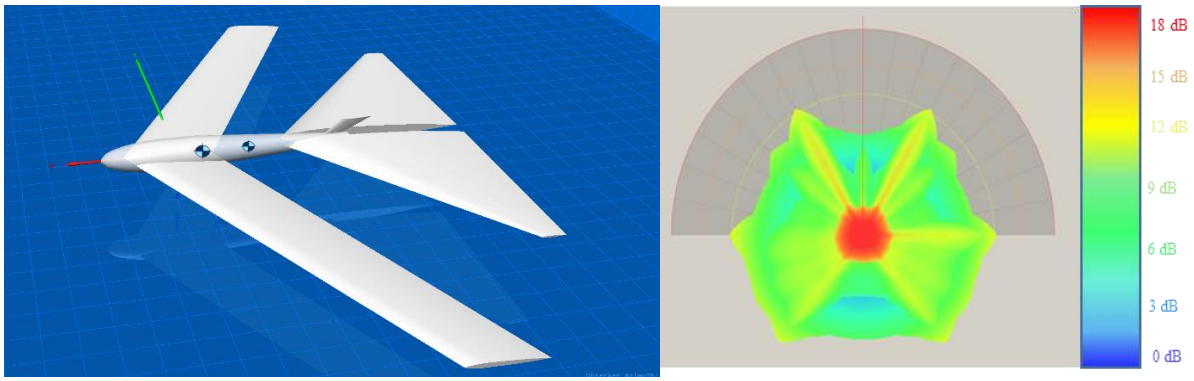


Figure 12 – Twentieth generation conceptual layout and radar signature visualization

Table 5 Conceptual layout and performance parameters

Layout Parameter	Value	Performance and Effectiveness Fitness Data	Value
Wingspan (b)	45(m)	Thrust-to-weight ratio	0.24
Wing Root Chord (c_0)	7.2(m)	Wing loading	598.36(kg/m^2)
Wing Tip Chord (c_1)	6.8(m)	Cruise speed	132.85(m/s)
Wing Leading-Edge Sweep Angle (α_1)	33(deg)	Fuel capacity	55119.28(kg)
Fuselage Radius (r)	2(m)	Fuel consumption rate	3.33(kg/s)
Fuselage Length (L)	23(m)	Effectiveness fitness score	0.75
Vertical Tail Area (S_V)	3.25(m^2)		
Horizontal Tail Area (S_H)	50(m^2)		

The simulation results of this generation showed that four enemy fighters were destroyed, three friendly fighters were lost, the bomber successfully survived, and successfully damaged the enemy target. From the perspective of flight performance, compared with the previous generation aircraft, the larger wing area of this generation aircraft effectively reduced the wing loading, while the dramatic reduction in vertical tail area significantly decreased the aircraft drag. From the perspective of stealth performance, the extremely small vertical tail area markedly reduced the lateral RCS of the aircraft, and thanks to the shielding effect of the wing on the fuselage, the aircraft initially acquired a certain degree of stealth capability. From the layout parameters and radar signature visualization characteristics, the flattened configuration substantially reduced the bomber's RCS value, greatly delaying the engagement distance with the enemy. However, due to the relatively large horizontal tail area, the bomber drag was relatively high, resulting in a lower flight speed and overall poor maneuverability. Nevertheless, the bomber successfully disengaged from the battlefield after completing the mission, leading to a significant improvement in the system-of-systems fitness score.

When the population evolved to the fiftieth generation, the final conceptual layout and radar signature visualization are shown in Figures 13. Its conceptual layout parameters and performance parameters are presented in Table 6.

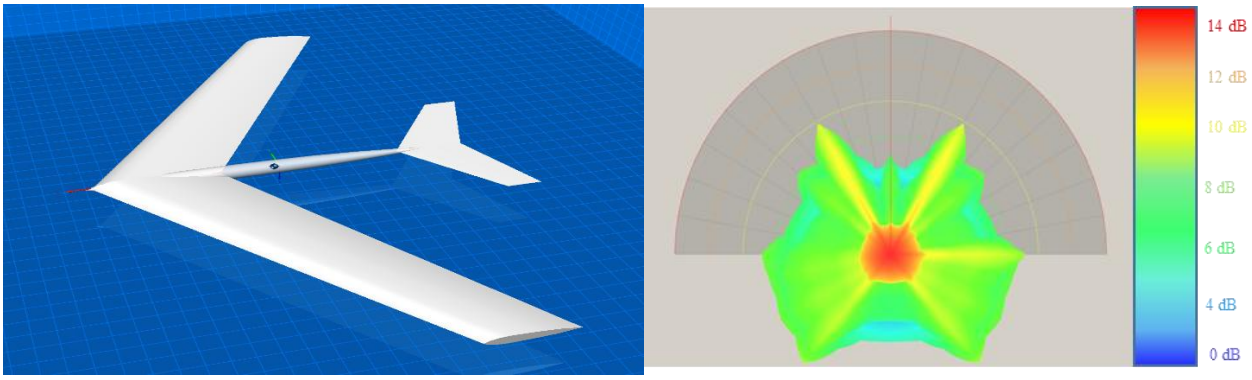


Figure 13 – Fiftieth generation conceptual layout and radar signature visualization

Table 6 Conceptual layout and performance parameters

Layout Parameter	Value	Performance and Effectiveness Fitness Data	Value
Wingspan (b)	30.48(m)	Thrust-to-weight ratio	0.29
Wing Root Chord (c_0)	5.48(m)	Wing loading	354.27(kg/m^2)
Wing Tip Chord (c_1)	3.66(m)	Cruise speed	243.91(m/s)
Wing Leading-Edge Sweep Angle (α_1)	35(deg)	Fuel capacity	53754.74(kg)
Fuselage Radius (r)	1(m)	Fuel consumption rate	3.39(kg/s)
Fuselage Length (L)	15.24(m)	Effectiveness fitness score	0.8
Vertical Tail Area (S_V)	0(m^2)		
Horizontal Tail Area (S_H)	10.46(m^2)		

The simulation results of this generation showed that four enemy fighters were destroyed, two friendly fighters were lost, the bomber successfully survived, and successfully damaged the enemy target. From the perspective of flight performance, compared with the previous generation aircraft, the larger wing area of this generation effectively reduced the wing loading, while the complete elimination of the vertical tail and the reduction in horizontal tail area significantly decreased the aircraft drag. From the perspective of stealth performance, the tailless vertical configuration and the smaller fuselage radius markedly reduced the lateral RCS of the aircraft, and thanks to the shielding effect of the wing on the fuselage, the aircraft achieved even better stealth capability. The excellent stealth performance enabled the formation to strike the outermost fighters first with a numerical advantage before the enemy could complete assembly; meanwhile, the bomber's flight speed of Mach 0.7 allowed the formation to rapidly disengage from the battlefield after completing the strike mission.

The cruise speed, the mean radar cross-section at 0° elevation and 0–40° azimuth, and the effectiveness fitness score data of the above conceptual layout schemes are summarized in Figure 14.

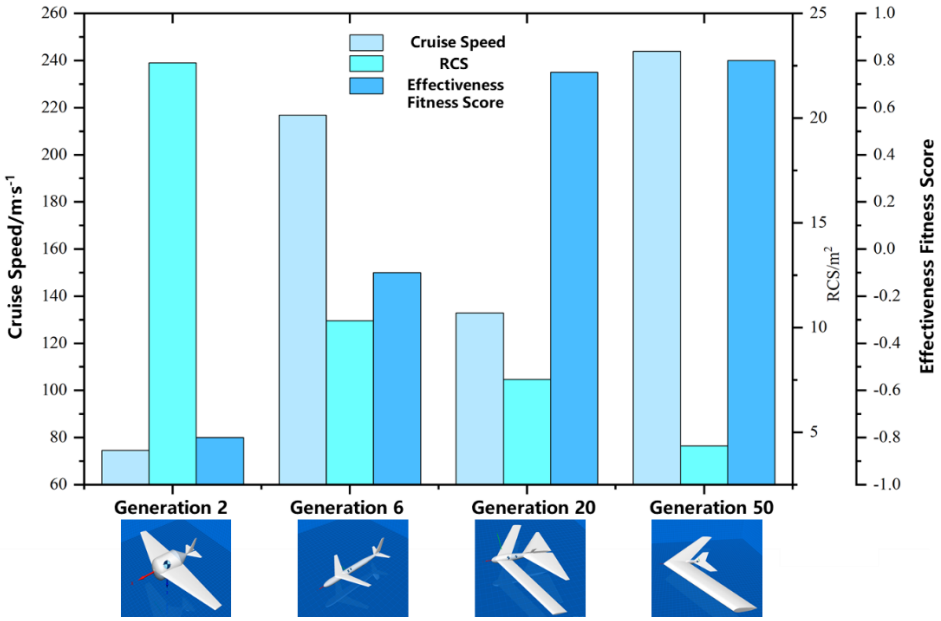


Figure 14 – Performance/effectiveness comparison of different aircraft conceptual layouts

From the graphical analysis, as the number of algorithm iterations increases, the conceptual layout of the bomber gradually optimizes towards a flattened configuration and exhibits a trend towards a flying wing layout. It can be observed from the charts that the dominant factor in the optimization process is stealth performance. As stealth performance is continuously improved, the algorithm constantly adjusts the layout parameters to enhance the aircraft's cruise speed, ultimately yielding a layout scheme with relatively superior flight performance and stealth performance. The progressively increasing effectiveness fitness score also verifies the adaptability of the layout scheme within this air combat system-of-systems.

4. Conclusion

To fully realize the cross-level closed-loop optimization between aircraft conceptual layout parameters and air combat system-of-systems effectiveness, this paper has primarily conducted the following research work.

1)An effectiveness-driven intelligent optimization method for aircraft conceptual layout is proposed. A cross-level optimization framework of "layout parameters – aircraft performance – system-of-systems effectiveness" is constructed, integrating parametric modeling, engineering empirical formulas, Agent-based system-of-systems effectiveness simulation, and an improved genetic algorithm, thereby forming a closed-loop process of "design – simulation – optimization."

2)A rapid estimation model for the flight performance and radar stealth performance of subsonic aircraft is established. Based on empirical formulas, the rapid calculation of key parameters such as cruise speed, fuel capacity, fuel consumption rate, and RCS is achieved. Meanwhile, an improved genetic algorithm mechanism is designed, featuring real-number encoding, a selection strategy combining elitism preservation and fitness-proportionate selection, uniform crossover, and an adaptive mutation operator.

3)A typical mission scenario of fighters escorting a bomber to conduct air-to-surface strikes is used as a case study for validation. The results show that the proposed method can converge within 50 generations, stealth performance dominates the optimization process, the final layout exhibits a flying-wing, tailless, and flattened trend, and the system-of-systems effectiveness score increases from a negative value to 0.8, thereby validating the feasibility and effectiveness of the method.

5. Contact Author Email Address

Wenzheng Liu: 1873120601@qq.com

6. Copyright Statement

The authors confirm that they, and/or their company or organization, hold copyright on all of the original material included in this paper. The authors also confirm that they have obtained permission, from the copyright holder of any third party material included in this paper, to publish it as part of their paper. The authors confirm that they give permission, or have obtained permission from the copyright holder of this paper, for the publication and distribution of this paper as part of the ICAS proceedings or as individual off-prints from the proceedings.

References

[1] Sproles, Noel. Formulating measures of effectiveness[J].*Systems Engineering*,2002,5,(4):253-263.

[2] Martins, Joaquim R. R. A.Lambe, Andrew B.Multidisciplinary Design Optimization: A Survey of Architectures[J]. *AIAA Journal*,2013,51,(9):2049-2075.

[3] Kano, Ryosuke,Ryuzono, Kazuki,Date, Shugo , et al.Conceptual design of composite aircraft using multidisciplinar y optimization[C].*//2025 AIAA SCITECH Forum*.2025:2025-0002.

[4] Wen Yao,Xiaoqian Chen,Wencai Luo , et al.Review of uncertainty-based multidisciplinary design optimization met hods for aerospace vehicles[J].*Progress in Aerospace Sciences*,2011,47,(6):450-479.

[5] Ahn, J.Kwon, J. H.An efficient strategy for reliability-based multidisciplinary design optimization using BLISS[J].*S tructural and Multidisciplinary Optimization*,2006,31,(5):363-372.

[6] Zhou J, Gong C L, Su H, et al. Optimal design problem of system of systems of flight vehicle[J]. *Acta Aeronautica et Astronautica Sinica*, 2018, 39(11): 97-109.

[7] Biltge Patrick Thomas Biltgen.A Methodology for Capability-Based Technology Evaluation for Systems-of-System s[D].*Georgia Institute of Technology*,2007.

[8] Liu Hu,Tian Yongliang,Gao Yuan , et al.System of systems oriented flight vehicle conceptual design: Perspectives a nd progresses[J].*Chinese Journal of Aeronautics*,2015,28,(3):617-635.

[9] Braafladt, Alexander C.Steffens, Michael,Mavris, Dimitri N.Tradespace Exploration and Analysis Using Mission Ef fectiveness in Aircraft Conceptual Design[C].*//AIAA Science and Technology Forum and Exposition (AIAA SciTec h)*.2020:535-548.

[10] Dietl, Tobias,Prakasha, Prajwal Shiva,Schmitz, Matthias , et al.Fighter Design and Fleet Effectiveness Evaluation via System of Systems Battlespace Simulation[C].*//AIAA Aviation Forum*.2023:20.

[11] Bi W H, Chen H, Wu Y X, et al. Architecture Design and Modeling of Manned/unmanned Cooperative Air Comb at Based on Complex Adaptive System Theory [J]. *Acta Armamentarii*, 2026, 47(1): 123-142.

[12] Macal, C. M.North, M. J.Tutorial on agent-based modelling and simulation[J].*Journal of Simulation*,2010,4,(3):15 1-162.

[13] Kuroswiski, Andre Rossi,Medeiros, Felipe Leonardo Lobo,De Marchi, Monica Maria , et al.Beyond visual range a ir combat simulations: validation methods and analysis using agent-based models[J].*The Journal of Defense Modeli ng and Simulation: Applications,Methodology,Technology*,2025,22,(4):387-404.

[14] Egbert Torenbeek,with a foreword by H. Wittenberg.Synthesis of Subsonic Airplane Design[M].*Springer Dordrec ht*,1982:XXII, 598.

[15] Zhiqi Liu,Mingqiang Luo,Yulu Ma , et al.A methodology for constructing the system-of-systems environment to e valuate UAV decision systems[J].*Defence Technology*,2026,56,(2):337-351.

[16] FENG Yimin,GE Ping,SHAO Yanli , et al.UAF-based integration of design and simulation model for system-of-s ystems[J].*Journal of Systems Engineering and Electronics*,2025,36,(1):108-126.

[17] Yu X Q. Multidisciplinary Design Optimization for Aircraft Conceptual and Preliminary Design:Status and Direct ions [J]. *Journal of Nanjing University of Aeronautics & Astronautics*, 2008(4): 417-426.

[18] Wu L, Zhang X Y, Dai Q Y, et al. Simulation and characteristic analysis of high speed craft RCS based on physica l optical method [J]. *Journal of Naval University of Engineering*, 2025, 37(3): 58-62.

[19] Wu G X, Deng W B, Jiang W. Rayleigh region partition and scattering characteristics of radar targets [J]. *Chinese Journal of Radio Science*, 2007, 22(3): 476-480.

[20] Zia Ud Din Taj,Ahmad Bilal,Muhammad Awais , et al.Design exploration and optimization of aerodynamics and r adar cross section for a fighter aircraft[J].*Aerospace Science and Technology*,2023,133,

[21] Smullen, Daniel,Gillett, Jonathan,Heron, Joseph , et al.Genetic Algorithm with Self-Adaptive Mutation Controlled by Chromosome Similarity[C].*//IEEE Congress on Evolutionary Computation (CEC)*.2014:504-511.

[22] Wei X F, Lou Z K, Tu Y, et al. Research on Kill Chain Analysis Method of Cooperative Combat Based on System of Systems Framework[J]. *Aero Weaponry*, 2025, 32(3): 31-39.

[23] Winkler, Luca,Strohal, Michael,Stuetz, Peter.Computer-Generated Forces Team Behavior within Air Combat Sim ulations: Interpreting Risks and Opportunities[C].*//2025 AIAA SCITECH Forum*.2025:2025-2791.